

Contents lists available at ScienceDirect

Fuel

journal homepage: www.elsevier.com/locate/fuel



Full Length Article

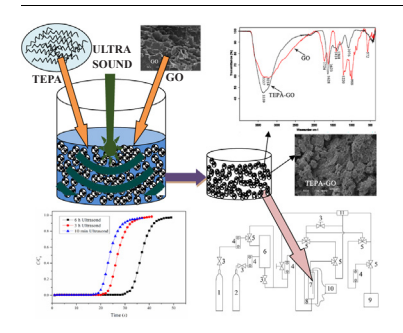
Ultrasound-assisted amine functionalized graphene oxide for enhanced CO₂ adsorption



Yamin Liu^{a,c,*}, Baharak Sajjadi^b, Wei-Yin Chen^b, Riya Chatterjee^b

- ^a School of Ecological Environment and Urban Construction, Fujian University of Technology, Fuzhou 350118, Fujian, China
- ^b Department of Chemical Engineering, University of Mississippi, MS 38677, USA
- ^c Fujian Indoor Environment Engineering Technology Research Center, Fuzhou 350118, Fujian, China

GRAPHICAL ABSTRACT



ARTICLE INFO

Keywords: Graphene oxide TEPA Amination Ultrasound Carbon dioxide Adsorption

ABSTRACT

The present study discusses a novel ultrasound promoted amination technique to functionalize graphene oxide (GO) for CO2 adsorption. Graphene oxide was synthesized following the modified Hummer's method. The developed functionalization technique integrates the advantages of low-frequency ultrasonic physical activation with the chemical functionalization using tetraethylenepentamine (TEPA). Acoustic treatment exfoliates the clusters of graphene oxide and enhances the surface area for the subsequent amine functionalization and CO2 adsorption. Changes in textural properties, surface functionalities, thermal stability, and elemental compositions were examined before and after activation of graphene oxide. The characterization results revealed substantial increment of N content, from 0.08 in pristine to 4.84% in functionalized GO and the subsequent reduction in surface area from 289 to $198\,\mathrm{m}^2/\mathrm{g}$ in the functionalized GO, indicating attachment of TEPA to GO structure. CO_2 adsorption experiments were conducted under diluted CO2 with the partial pressure of 0.10 atm. at 338 K and the results revealed that ultrasonic-TEPA activated GO possessed enhanced adsorption capacity of 1.2 mmol g⁻¹ over pristine GO. While pristine GO could only achieve the maximum adsorption capacity of $0.3\,\mathrm{mmol\,g}^{-1}$ at 303 K. Besides, the sonochemically modified adsorbent showed stable cyclic adsorption-regeneration performance with only 1% reduction in adsorption capacity after 10 cycles. Finally, the effectiveness of the developed physicochemical activation technique was determined by comparing its adsorption capacity with the adsorbents found from literature.

^{*} Corresponding author at: School of Ecological Environment and Urban Construction, Fujian University of Technology, Fuzhou 350118, Fujian, China. E-mail address: mingjing2000@126.com (Y. Liu).

1. Introduction

The recent studies by the world's energy landscape revealed that the fossil fuels (such as petroleum, natural gas etc.) are still the world's primary energy sources that provide 65% of the total energy output. This trend is expected to continue for the coming 100 years as well [1,2]. Under such circumstances, the wide applications of CCS (Carbon Capture and Storage) is an important component of the long-term goal of reducing the anthropogenic CO₂ emissions [1,3]. Among several CCS technologies, post-combustion CO2 capture could be very effective in reducing the elevated anthropogenic CO2 concentrations. The postcombustion-based technologies mainly include liquid amine/ammonia absorption, porous materials adsorption, and membrane separation. Among these, the porous material adsorption technology has drawn wide attention in recent years due to its potential to meet the requirements of energy-efficiency and cost-effectiveness CO2 remediation [4-6]. However, synthesis of efficient solid adsorbents is the major concern. The recent studies have shown that zeolites [7], mesoporous silicon [8,9], metal-organic frameworks (MOFs) [10], carbon materials [11-14], pillared lamellar clays [15], and the polymeric amine containing hybrid adsorbents are effective solid CO₂ adsorbents [16,17]. However, the industrial applications of these new adsorbents are limited due to several reasons. For instance, the physical adsorbents (like zeolites, molecular sieves etc.) usually have a low adsorption capacity at elevated temperature (actual flue gas temperature) and the chemical adsorbents (mainly amine-functionalized porous materials) often suffer from the costly and complex preparation processes and also structural instability [18]. Therefore, a wide range of studies has been carried out to synthesize efficient and inexpensive adsorbents. Materials with a high surface area, high porosity and active surface functionalities (e.g. activated carbon, biochar, graphene oxide) are promising precursors for synthesizing effective adsorbents [13].

Graphene oxide (GO) which has high crystallinity and electronic quality, is emerging rapidly as a potential candidate in the field of carbon capture. GO is the functionalized graphene derived from the oxidation of graphite in presence of strong oxidizing agents and consists of two dimensional sp² bonded carbon honeycomb lattice structure ref. The oxidation resulted in the enhancement of the interlayer spacing of the graphene layers and makes it hydrophilic [19]. Many of the earlier structural models of GO have proposed regular lattices composed of discrete repeat units [20]. For instance, the structural studies by Hofmann and Holst [21], revealed that GO consists of oxygen-containing chemical groups; such as hydroxyl and carboxyl on its edges and epoxy on basal plane [20]. These oxygen functional groups are highly susceptible to chemical modification especially with nitrogenous compounds such as amine. Therefore, the surface modification of GO with amines or amine-containing molecules takes place very efficiently through nucleophilic substitution reactions. Graphene oxide (GO) has been used as a potential CO₂ adsorbent due to its surface functionality, large specific surface area, porosity and high thermal and chemical stability [22,23]. The oxygen functional groups on the surface of the GO makes it basic in nature. On the other hand, CO2 is acidic so its interaction with the basic adsorbents helps to achieve high CO2-capture capacity [22]. Moreover, the hydrophilicity of the GO makes it easily solvable in aqueous solution to yield mono, bi, or few-layers of GO sheets with stable dispersions [24]. This eventually enhances the surface area for adsorption and provides a more number of active sites for further surface modification [24]. Apart from the CO₂ sequestration, graphene oxide has several other applications like manufacturing of supercapacitors, fuel cells, and photovoltaic cells etc. and has immense importance to the scientific research community [25]. While graphene oxides have triggered tremendous technological and scientific interests, its potential application in CO₂ sequestration remains limited due to its low adsorption capacity [24]. Therefore, GO needs further modifications to improve its adsorptive capacity. The carboxyl, hydroxyl and epoxy groups of GO act as active sites for further surface modifications primarily through the basic moieties like amines or ammonia. Amines are nucleophilic, so can interact strongly with electrophilic CO2 through nucleophilic substitution reactions to provide improved CO₂ adsorption capacity. For instance, ethylenediamine (EDA) functionalized graphene oxide showed selective adsorption of CO₂ with an CO₂ adsorption capacity of 1.1 mmol g^{-1} of sorbent [26]. However, the chemical functionalization may be hindered since the graphitic clusters tend to agglomerate in presence of water, blocking the pores that are active sites for CO₂ adsorption. To overcome this problem, GO needs to be mixed homogeneously into the water through ultrasonic irradiation that can prevent the formation of an agglomerated graphitic sheet. Under Ultrasound irradiation, graphene layers can be completely exfoliated into graphitic and graphene oxide clusters [27,28] resulting in the enhancement of surface area and surface functionality of the graphene platelets. Low-frequency ultrasound induced cavitation phenomenon, which includes the three steps of nucleation, growth, and collapse of micro-bubbles filled with liquid vapor. Implosion (or collapse) of micro-bubbles produce microjets, shock waves, microstreaming and hot spots that lead to the excitation of the GO clusters through the formation of empty pores and creating the active sites for further chemical functionalization which subsequently provide the enhanced adsorptive capacity. Previous work by our group [27] demonstrated that polyaromatic hydrocarbons (PAH) of biochar structure went under reductive photo-carboxylation and its hydrogen content was magnified up to 24% that in turn increased its energy content up to 50% Additionally, it also showed that biochar was exfoliated into graphene oxide clusters under ultrasound irradiation that enhanced the reactivity of edge carbons of these platelets. This was further corroborated in our phyisico-chemical activation work. Biochar with exfoliated basic graphene oxide clusters is expected to be more susceptible to chemical modification since more surface is available for modification. This was further demonstrated in our subsequent work of physicochemical activation of biochar for efficient CO₂ adsorption which showed the ultrasound treatment facilitated the chemical activation significantly [29].

Although, the gas adsorption properties of graphite/graphene oxide have been studied by several research groups [30–32]. There are very less studies on the adsorption of CO_2 using functionalized GO (FGO). Besides, only few researches have been conducted to determine the effects of the amine compound and modification conditions on CO_2 adsorption using FGO. Aminated graphite oxide possessed higher CO_2 adsorption capacity than pure GO owing to specific interactions between amino groups and CO_2 [26]. This trend was also observed in our previous work on efficient ultrasono-amine functionalization of biochar for CO_2 removal [29]. The work revealed that CO_2 can be attached to the edge carbons of biochar consisting of reactive oxygen functionalities. This interaction was further boosted during ultrasono treatment where reactivity and surface area of biochar structure was enhanced to cater the attachment of the amine groups. Thus, the ultrasound treated and amine activated biochar provided as an attractive sorbent to capture CO_2

Therefore, the present study aims at synthesizing amine functionalized GO (AFGO) and investigating its effect on the CO_2 adsorption. To achieve this, GO was first synthesized from graphite flakes following the improved Hummers method and was aminated by an integrated physical activation and amine grafting technique under ultrasound irradiation. TEPA was selected among several other amines because of its low cost, low toxicity and the reasonable number of $-\mathrm{NH}_2$ groups that can improve the adsorption of CO_2 .

2. Materials and methods

2.1. Materials

Graphite flakes (Asbury Graphite Mills, Inc.), sulfuric acid (98%, Sigma Aldrich), sodium nitrate (Sigma Aldrich), potassium

permanganate (Sigma Aldrich), Hydrogen peroxide (30%, Sigma Aldrich), hydrochloric acid (37%, Sigma Aldrich), ethanol (Sigma-Aldrich.), distilled water (Fisher Scientific) were used for synthesis of GO. Methanol (Sigma-Aldrich), N-(3-dimethylaminopropyl-N'-ethylcarbodiimide hydrochloride (EDC 98% purity, Sigma Aldrich), hydroxybenzotriazole (HOBt, 97% purity, Sigma Aldrich), tetraethylenepentamine (TEPA, Sigma Aldrich), sodium hydroxide (Fisher Scientific), and acetone (Sigma-Aldrich) were used for the amine functionalization of the GO surface. All chemicals used were of analytical grade.

2.2. Sample preparation

2.2.1. Synthesis of GO

GO was prepared according to the improved Hummers' method as reported by Marcano et al. [33]. In this method, the formation of GO from graphite constitutes three distinct independent steps: the conversion of graphite into a graphite intercalation compound (GIC), conversion of the GIC into oxidized graphite (pristine graphite oxide or PGO) and finally, conversion of PGO into GO after exposure to water. The second step is the rate-limiting step that involves the diffusion of the oxidizing agent into the preoccupied graphite structure and makes the entire process diffusive-controlled [34].

To synthesize GO, at first, the concentrated H₂SO₄ solution (69 mL) was added to a mixture of graphite flakes (3.0 g, 1 wt equiv.) and NaNO₃ (1.5 g, 0.5 wt equiv.), meanwhile, the mixture was cooled to 273 K using an ice bath. Then, KMnO₄ (9.0 g, 3 wt equiv.) was slowly added to the mixture in portions to keep the reaction temperature below 293 K. After that, the mixture was warmed to 308 K and stirred for 7 h. The additional KMnO₄ (9.0 g, 3 wt equiv.) was then added to the reaction mixture and stirred for 12 h at 308 K. The reaction mixture was cooled to room temperature and poured onto ice (Ice mixture) (\sim 400 mL) with 30% H₂O₂ (3 mL). The mixture was sifted through a metal U.S. Standard testing sieve (300 µm), centrifuged (10,000 rpm for 20 min) and the supernatant was decanted away. The remaining solid material was washed sequentially with 200 mL of water (Distilled water), 200 mL of 10% HCl, and 200 mL of ethanol (2 times). For each wash, the mixture was centrifuged at 10,000 rpm for 20 min. Finally, the solid obtained after repeated washing was dried overnight under vacuum at room temperature.

2.2.2. Preparation of amine functionalized graphene oxide (AFGO)

The functionalization of graphene oxide is a combined two-step process consists of physical activation by ultrasound and chemical activation with TEPA. Physical modification of biochar was achieved under 20 kHz low frequency ultrasound irradiation (Sonicator model no. XL2010 with maximum power of 475 Watts). The applied ultrasound during the physical activation induced cavitation that exfoliated the graphene layers and enhanced the reactivity of the surface functional groups. This further helped in grafting TEPA during the functionalization step.

In a typical experiment, 10 mg of GO substrate was suspended in 30 mL of distilled water and sonicated for 15 min. EDC and HOBT each of 25 mg were added and the mixture was sonicated for 1 h, then stirred at 313 K for 24 h followed by centrifugation. EDC-HOBt were used as coupling agents to activate the surface —COOH group of GO prior to amine functionalization. To attain maximum activation of carboxyl groups, equal amount of EDC and HOBt is required. This can be further substantiated from the mechanism of GO functionalization that has been explained in Section 2.5. The solid material left after centrifugation was suspended in methanol (50 mL), sonicated for 30 min and then 100 mg of amine (TEPA) was added to the mixture. After 6 h of sonication, the mixture was stirred at room temperature for 24 h, centrifuged and the supernatant was decanted away. The remaining solid was then first washed with distilled water twice followed by 1 N NaOH, 1 N HCl (aq.) and acetone. For each wash, the mixture was centrifuged

at $10,000\,\mathrm{rpm}$ for $20\,\mathrm{min}$ and the supernatant was discarded. The solid obtained from the last centrifugation was vacuum dried overnight at room temperature.

2.3. Characterization

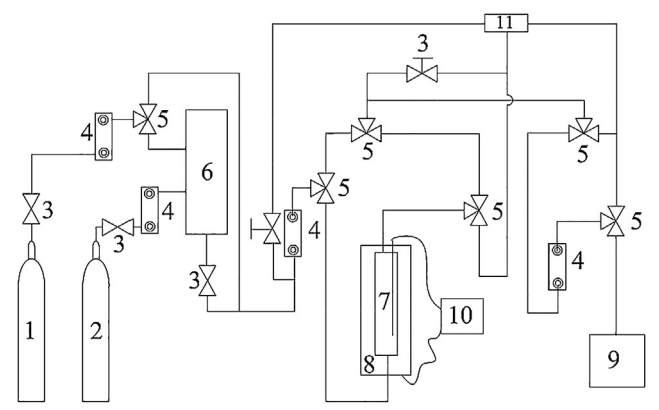
The surface crystallinity of the activated graphene oxide was determined from the XRD analysis in a Rigaku powder diffractometer (Rigaku, Japan) with Cu K α radiation ($\lambda = 0.15406$ nm). The tube voltage was 45 kV, and the current was 40 mA. The XRD diffraction patterns were taken in the 2θ range of 5–60° at a scan speed of 2°/min. Surface morphology was determined with a scanning electron microscope (JSM-5600 Scanning Electron Microscope, JEOL USA Inc. Peabody, MS). The effects of ultrasound and chemical functionalization on the porosity and the surface area were investigated by the nitrogen adsorption/desorption isotherms in Quantachrome 2000E series surface area analyzer. The sample was degassed at 573 K under nitrogen flow for 3 h prior to measurement. Surface area was calculated using the Brunauer-Emmett-Teller (BET) equation. Pore size distributions were determined by the Barrett-Joyner-Halenda (BJH) method. Total pore volume was calculated from the amount of adsorbed N_2 at $P/P_0 = 0.99$. Thermal stability of the prepared adsorbent was measured using the thermal gravimetric analysis that was carried out using a TG (SDT Q600, TA Instruments) device under dynamic N2 atmosphere at temperature ranging from 303 K to 973 K with a heating rate of 10 K/min. The surface functional groups and the chemical species of the adsorbent were examined using Raman (LabRam HR Evolution at a range of $400-4000\,\mathrm{cm}^{-1}$ at an excitation wavelength of 633 nm) and Fourier Transform Infrared (FTIR, Cary 660 FTIR Agilent) spectroscopies. Elemental analysis (C, H, N and ash, using ICP-MS Analysis) results were provided by the Huffman Hazen Laboratory (Colorado, USA).

2.4. Adsorption/desorption studies

2.4.1. Adsorption of CO₂

The experimental setup for $\rm CO_2$ adsorption is depicted in Fig. 1. The adsorption column was made of alumina oxide and was 40 cm in length with 1.5 cm inner diameter. This was placed in a temperature-controlled furnace (Lindberg). The column was connected to an adjusting tank through the upstream and a $\rm CO\text{-}CO_2$ analyzer (ZRH Infrared analyzer) through the downstream. The adjusting tank mixed the $\rm CO_2$ gas with the inert gas (He with 99.99% purity) at the desired concentration and introduced the flow to the adsorption column. The $\rm CO\text{-}CO_2$ analyzer then measured the concentration of $\rm CO_2$ after exposing to the adsorbent.

In a typical experiment, 1.0 g of AFGO (the adsorbent) was placed



1: Helium 2: Carbon dioxide 3: 2way valve 4: Flow meter 5: 3 way valve 6: Mixture tank 7: Adsorption column 8: Furnace 9: CO2 analyzer 10: Temperature Controller 11: Vent

Fig. 1. CO₂ adsorption experiment setup.

inside the column and degassed at a temperature of 378 K under helium flow of $500\,\mathrm{cm^3}$ min $^{-1}$ for 1 h and then, cooled to 338 K. Once the temperature reached to 338 K, the helium flow was immediately switched to a $\mathrm{CO_2}$ -containing simulated flue gas at the same flow rate. After the flow was stabilized, the analyzer recorded the desired inlet $\mathrm{CO_2}$ concentration, which was maintained at 10 vol%. After achieving the stable inlet concentration, the flow was directed towards the adsorption and the $\mathrm{CO-CO_2}$ analyzer respectively. Finally, the adsorption capacity was calculated based on the concentration differences between the inlet and outlet using the following equation.

$$q_a = \frac{1}{M} \times \left[\int_0^t Q \times \frac{C_0 - C}{1 - C} dt \right] \times \frac{T_0}{T} \times \frac{1}{V_m}$$
 (1)

where q_a is the adsorption capacity of CO₂, mmol g⁻¹; M is the weight of adsorbent, g; Q is the gas flow rate, cm³ min⁻¹; C_0 and C are influent and effluent CO₂ concentrations, vol.%; t represents the time, min; T_0 is 273 K, T is the gas temperature, K; and V_m is 22.4 mL mmol⁻¹.

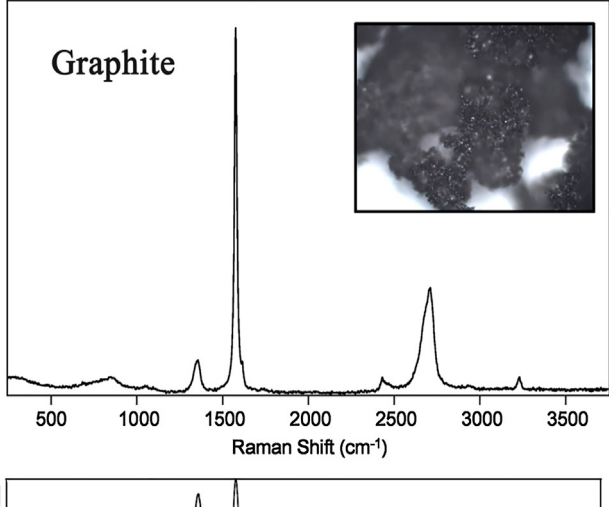
2.4.2. Desorption of CO₂

The desorption experiment was carried out in the same experimental system. In a typical experiment, the adsorption column containing the adsorbent was heated to the desired regeneration temperature (378 K) and then the gas was switched to pure helium flow. At the same time, the online CO-CO_2 analyzer measured the CO_2 concentration of outlet gas. The total amount of CO_2 was calculated based on the CO_2 concentration and the helium flow rate.

2.5. Mechanism of amine functionalization of graphene oxide

In this study, coupling method was followed for the amination of graphene oxide. In this method, the amine functionalization takes place through the conversion of a —COOH (carboxyl) group of GO surface to a —CONHR (amide) group, where R contains an amine group. Prior to this, the —COOH group needs to be activated to react with an amine. As shown in the Fig. 2, coupling agents of EDC-HOBt was used for the activation of carboxyl group. In this process, at first, EDC reacts with the carboxylic acid group and forms O-acylisourea as an intermediate which is replaced by the nucleophilic attack from the amino groups in the reaction mixture, producing amide and releasing iso-urea as a

Fig. 2. Chemical functionalization of graphene oxide with TEPA.



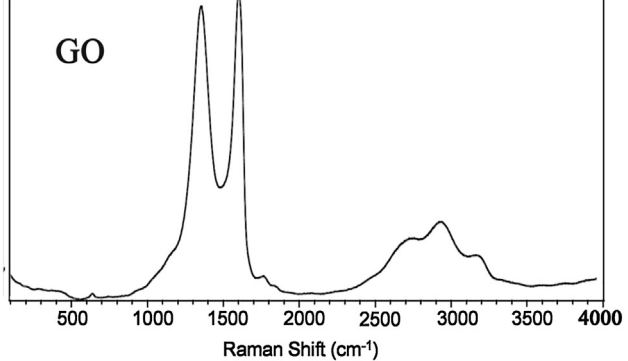


Fig. 3. Raman spectra of graphite and graphene oxide powders.

byproduct [27,33]. However, there is a possibility of a side reaction to occur forming an N-acyl urea. Incorporation of appropriate additives such as HOBt prevents this side reaction effectively [29]. Finally, the amination is achieved by the nucleophilic substitution of the activated carboxyl group with TEPA to form AFGO. After the completion of the reaction, isolation of products from the unreacted reagents can be done easily by simple filtration.

3. Results and discussions

3.1. Raman spectra of graphite powder and GO powder

Fig. 3 represents the Raman spectra of graphite and GO powder. The Raman spectrum of graphite powder displayed an intense G peak at 1580 cm⁻¹, a D peak at 1336 along with the weak 2D peak at 2800 cm⁻¹. The D peak corresponds to the first order scattering of the tangential stretching $(E_{2g})[35]$ mode from the disorder in the planar sp²-hybridized carbon network. In other words, it represents the impurities and defects associated to the graphitic structure. The G peak represents the hexagonal layered crystal structure of graphite with the trivalent carbon atoms grafted in the lattice to form a two-dimensional honeycomb network [35]. The intensity of D peak increases as more defects are added (particularly in form of activation) to the structure [36]. Therefore, the less intense D peak substantially confirmed the precursor material used in the present study was a pure form of graphite. The other low intensity peak at 2800 cm⁻¹ corresponds to the signature peak of graphitic sp² structure and found mostly in the carbonaceous materials that are composed of the graphitic clusters (such as biochars) [37]. Further, the Raman spectrum of GO, exhibited much intense D peak than the pure graphite. This clearly reflected the characteristics of the lattice distortion in the graphene sheets (presence of D bands) as a result of activation. This was also highlighted by Nakamizo

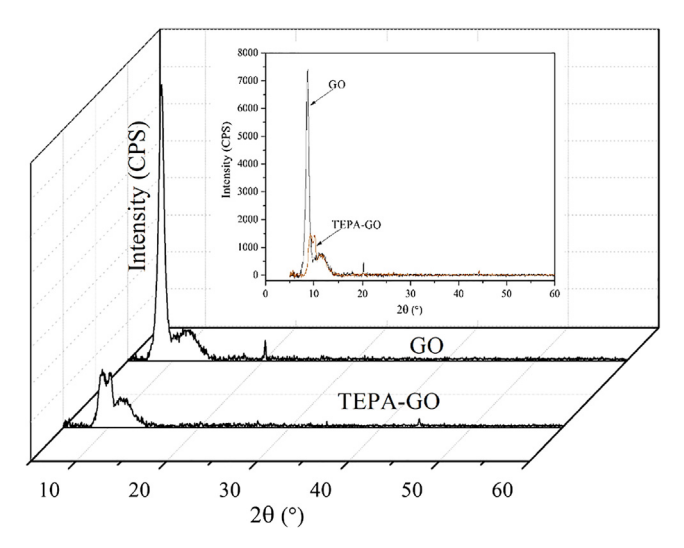


Fig. 4. XRD patterns of GO and TEPA-GO.

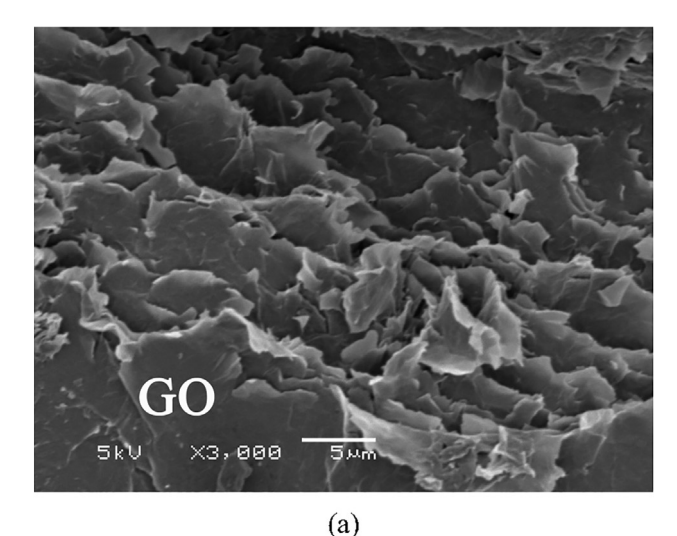
et al. where they observed pure graphite consists of strong G peak and weak D peak. However, upon distortion of the lattice structure, the D peak became intense [38]. In addition to that, the Raman spectrum of GO powder also showed a broadened G peak shifts to 1599 cm⁻¹, whereas the D peak became the most obvious that appeared at 1341 cm⁻¹, suggesting the destruction of the graphite sp² structure and formation of the sp³ bonds in the carbon network [39]. The observed differences between the spectrums could be attributed to the amorphization of graphite during GO formation. These results are consistent with the literature reported by Oh et al. [39]

3.2. XRD analysis

XRD pattern of GO and TEPA-GO powder are shown in Fig. 4. The spectrum for GO reveals a strong peak at $2\theta = 8.9^{\circ}$ that corresponds to the GO (001) crystal face and consistent with the patterns of GO reported in the literature [40]. This peak partially overlaps with the peak at 11.0°, indicating that the crystal structure is not perfect because GO still has a laminated structure [26,41]. As observed from the figure that the degree of the Bragg's diffraction angle slightly increases for TEPA-GO (10.1°) than GO (8.9°). This can be attributed to the disorder associated with the addition of amines to the exfoliated and oxidized graphitic structure under basic activation conditions [42]. The reduction of the intensity of the diffraction peak for TEPA-GO (compared to GO) also demonstrates that TEPA was successfully grafted onto the porous wall of graphene oxide. Furthermore, the literature suggests that the XRD patterns become weak or even disappear if GO is cross-linked at either edge or side of the sheets and its regular stacks are destroyed [43]. As observed from the Fig. 4, after incorporation of TEPA, the intense peak disappeared, indicating that the introduction of amine prevented the restacking of GO sheets. Similar observation was also reported by Sui et al. when they grafted PEI polymer to the graphene oxide matrix [43]. Besides, the XRD pattern of TEPA-GO depicts the presence of two small peaks (9.3° and 10.1°) apart from the characteristic peak (8.9°) of GO. This further indicates that the structure of TEPA-GO powder is amorphous, and the internal crystal is not as regular as GO [26]. This can be explained as the effect of chemical grafting and formation of a strong bond between the GO and TEPA that created additional defects on the GO surface, thereby weakening the structure of the GO [44].

3.3. SEM results of GO and TEPA-GO

The surface morphology of GO and TEPA-GO is shown in Fig. 5a-b. The GO exhibited a folded structural feature consisting of multilayered



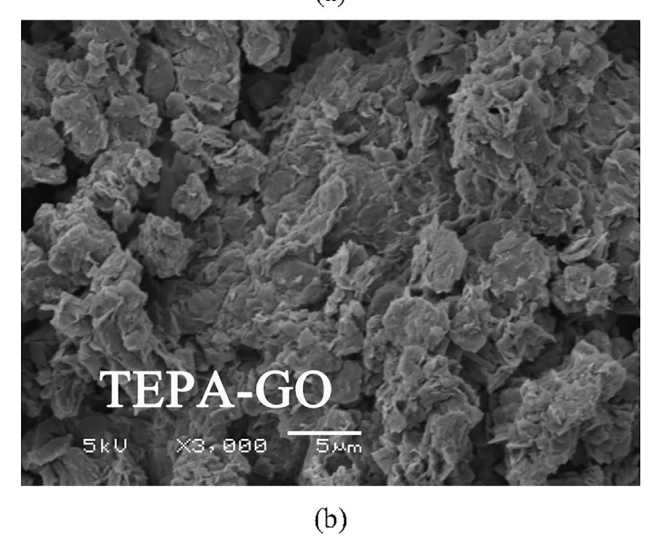


Fig. 5. SEM images of (a) GO powder and (b) TEPA-GO powder.

lamellas. The SEM image from Fig. 4a also revealed the fractured structure of graphene oxide with well-packed layers through almost the entire cross-section of the sample [45]. This kind of surface morphology was attributed to the result of oxidation of graphite cluster. While this did not necessarily signify that all of the stacking of the graphite cluster were destroyed, it indicated that any remaining stacking was disordered [46]. The disruption of the structure due to oxidation reduced the attractive interactions between the layers, allowing the material to be easily dispersed in solvents [46]. This facilitated the subsequent dispersion of GO for the TEPA functionalization. The SEM image of TEPA-GO (Fig. 5b) revealed that the functionalized graphene material consisted of randomly aggregated, thin, crumpled sheets closely associated with each other and forming a disordered and dense solid structure [45]. The SEM image of TEPA-GO also demonstrated that the amine was coated throughout the surface as a result of chemical functionalization [29]. This resulted to the reduction of surface area and pore volume of the structure which was further verified in terms of BET surface area analysis. The structural differences between GO and TEPA-GO was due to the fact that TEPA chemical grafting onto the GO surface resulted in additional defects in the GO surface, which led to the destruction of the GO stable layered structure and the formation of dense porous morphology. These observations were consistent with the XRD results discussed before.

Table 1
Textural properties of GO and AFGO using N₂ as adsorption at 77 K.

Samples	Surface area (BET) (m ² /g)	Pore volume (cm ³ /g)	Pore diameter (BJH) (nm)
GO	289.028	0.046	19.117
TEPA-GO	194.484	0.042	16.938

3.4. BET analysis of GO and TEPA-GO

The textural properties of GO and TEPA-GO, including the surface area, average pore diameter and pore volume were characterized by nitrogen adsorption at 77 K, and the results were summarized in Table 1. Based on the IUPAC classification, adsorption pores can be classified into three groups: micropore (diameter < 2 nm), mesopore (2 nm < diameter < 50 nm) and macropore (diameter > 50 nm) [47]. Surface area analysis demonstrated that GO and AFGO consisted of mesopores. Besides, it was observed that the surface area, average pore diameter and pore volume of GO reduced after TEPA activation (Table 1). This can be explained based on the combined effect of ultrasound and amine functionalization. Longer duration of sonication induced intensified cavitation that affects the orientation of the graphene sheet and disarranged the layered structure consequently reducing the surface area. Moreover, the grafting of the amine to the GO matrix formed a layer on the surface which resulted in further reduction of the surface area and pore volume. Thus, the reduced value of surface area and pore volume of aminated graphene oxide substantially demonstrated the attachment of amines to the GO structure. This can be further substantiated based on the literature on functionalized graphene oxide where it was mentioned that N-doped graphene oxide showed lower values of surface area compared to its precursor [43].

3.5. TGA of GO and TEPA-GO

The thermal behavior of GO and TEPA-GO was studied by TG analysis, as shown in Fig. 6. Two regions of mass loss were found in TG curves of both the GO and TEPA-GO. The first mass loss zone (both GO and TEPA-GO) was between 293 K and 423 K with a mass loss of about 15% as a removal of adsorbed water and $\rm CO_2$ [27]. For the GO, the second decomposition occurred at 423 K with 85% mass loss and was attributed to the rapid thermal degradation of GO. For TEPA-GO, the second mass loss zone was observed at the temperature range of 423–673 K with a value of about 35% due to the decomposition of amine groups [26]. These results suggested that the TEPA-GO was thermally stable at a temperature of 423 K. The thermal resistance

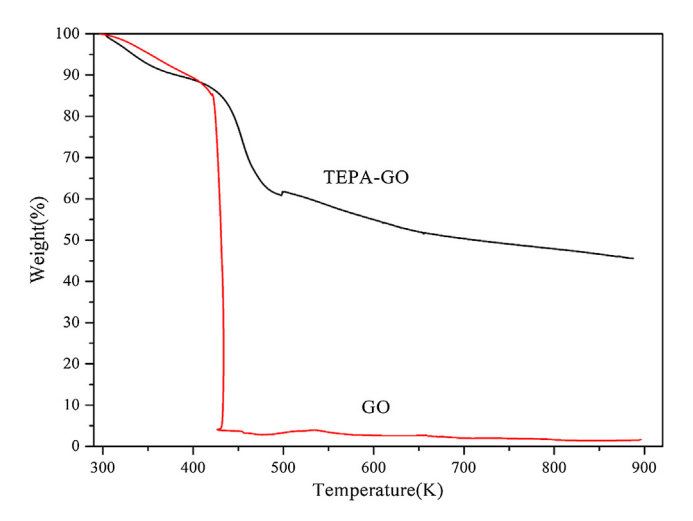


Fig. 6. TGA results of GO and TEPA-GO.

Table 2Elemental analysis of GO and TEPA-GO.

Samples	C	N	O	S	Ash
	% w/w				
TEPA-GO	52.68	4.84	14.66	1.15	25.32
GO	62.17	0.08	20.24	9.59	4.73

Table 3Elemental compositions GO and TEPA-GO based on organic components (omitting ash contribution).

Samples	C	N	O	S
	% w/w	% w/w	% w/w	% w/w
TEPA-GO	70.54	6.48	19.63	1.54
GO	65.26	0.08	21.24	10.07

property of aminated GO makes it ideal candidate for CO_2 adsorption from flue gas since the flue gas temperature (373 K) is well below the thermal stability range of AFGO. The thermal stability of the produced TEPA-GO, in other words, showed that the efficacy the physico-chemical activation technique developed in the current study.

3.6. Elemental analysis of GO and TEPA-GO

Table 2 describes the elemental compositions (N, C, O, S and ash) of GO and TEPA-GO. Besides, the pure organic compositions of both the samples were calculated with omitting ash contribution as tabulated in Table 3. As observed from both the tables, the N content of TEPA-GO (4.84%) was almost 60 times higher than that in pure GO (0.08%), confirming the significant quantity of amine attached to GO during functionalization. This further evaluated the effectiveness of TEPA, which is a rich source of nitrogen (37%) with 5 amine groups. Additionally, the activation method also proved to be very effective in enhancing the nitrogen content of the sorbent in presence of the amine.

As observed from Table 2, the ash content was enhanced significantly after functionalization. The similar phenomenon was observed in our previous work where biochar was functionalized following the similar sono-chemical activation technique [29]. Besides, the %C content of the TEPA-GO reduced after amination if the ash contribution is taken into consideration. However, when the ash was omitted it showed the gain in %C. This can be explained as when ash was omitted during the calculation of pure organic components, its effect was balanced by the carbon so %C content was enhanced. This observation further shows the significance of pure organic composition analysis without taking into consideration the ash content. The reduction of %O content is also consistent since the interaction between amine and GO resulted to the conversion of -COOH group to -CONH group and reducing the oxygen functionalities. The amount of sulfur reduced in functionalized GO which suggests that the ultrasound-amine combined treatment could help lead to the production of sulfur-free, cleaner adsorbent. Therefore, it could be concluded that the physicochemical treatment helped in improving the quality of the adsorbent for its application in CO₂ adsorption except the ash content. This opens a new avenue to direct our future study to apply the ultrasound effectively for the reduction of the ash content.

3.7. FTIR of GO and TEPA-GO

The FTIR spectrums of GO and TEPA-GO are shown in Fig. 7. For GO, the characteristic peaks at 1220 and 988 cm⁻¹ confirmed the presence of the epoxy groups complying with the symmetric stretching and deformation vibrations [39]. Besides, the peaks at 1724, 1414 and 1623 cm⁻¹ appeared due to the C=O, C-O and aromatic C=C stretching vibrations [48]. Further, the broad absorption peak was

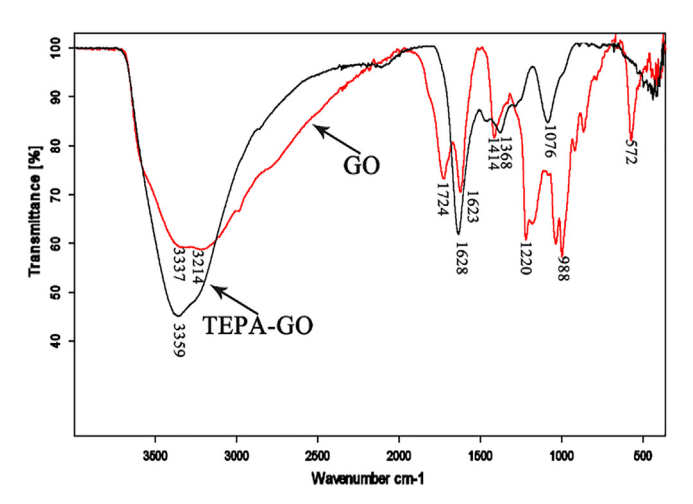


Fig. 7. FTIR spectrums of GO and TEPA-GO.

observed at 3214-3337 cm⁻¹ due to the O-H stretching vibration and the absorbed water molecules. Although the structure of the FTIR spectrum of the TEPA-GO remained the same, some new peaks appeared due to the chemical functionalization. For instance, the first obvious change was observed in the peak at 3359 cm⁻¹ due to the amine attachment. The N-H peak was found to be intense in the functionalized amine structure due to the N-H bending and N-H wagging vibrations [48]. Further, the peaks at 1724 and 1623 cm⁻¹ (related to C=O and C=C stretching) for GO disappeared due to the interaction between GO and TEPA. Instead a peak at 1628 cm⁻¹ appears for the functionalized sorbent due to the formation of -CONH bond as a result of amine activation [26]. Hence, these results suggested the chemical grafting of amine in and onto the GO structure. In addition to that the peak corresponding to the -OH deformation at 1368 cm⁻¹ was generated due to the attachment of amine to the oxidized graphite matrix [49]. Moreover, the assumption of reduction of the oxygen functionalities and its conversion to amide as a result of functionalization was consistently observed from the IR spectrum. For instance, at 1076 cm⁻¹ a peak appeared that corresponds to the C=O group after the disappearance of the two oxygen functional groups at 1220 and 988 cm⁻¹ which could be solely attributed to the result of amine functionalization [50]. Therefore, the FTIR analysis showed the effective amine grafting to the GO to produce suitable sorbent for CO2 capture.

3.8. The adsorption capacity of TEPA-GO

The dynamic CO_2 adsorption experiments were carried out at 338 K with (inlet CO_2 concentration) $C_0=10\,\mathrm{vol}\%$ CO_2 . The adsorption breakthrough curves of three different sonication treatment time are shown in Fig. 8 and the CO_2 adsorption capacities of GO and TEPA-GO are presented in Table 4.

The abscissa in Fig. 8 represents the time and the ordinate denotes the ratio of CO_2 concentration of the inlet and outlet gas. The overall breakthrough profiles for the three different sonication durations showed similar adsorptive behavior. As observed from the Table 4, the adsorption capacities of pristine graphene oxide (at different temperatures) are very limited. Besides, as temperature was increased from 303 K to 338 K the sorption capacity was reduced significantly. This can be explained based on the exothermic behavior of the adsorption phenomenon. Although lower temperature favored the CO_2 adsorption, the experiments with the activated GO was conducted at higher temperature (338 K) to determine the thermal stability and reactivity of the sorbent at elevated. The prepared AFGO showed increasing trend of the adsorption capacity with the sonication duration. Therefore, it can be affirmed that the ultrasound irradiation had a dominant effect that

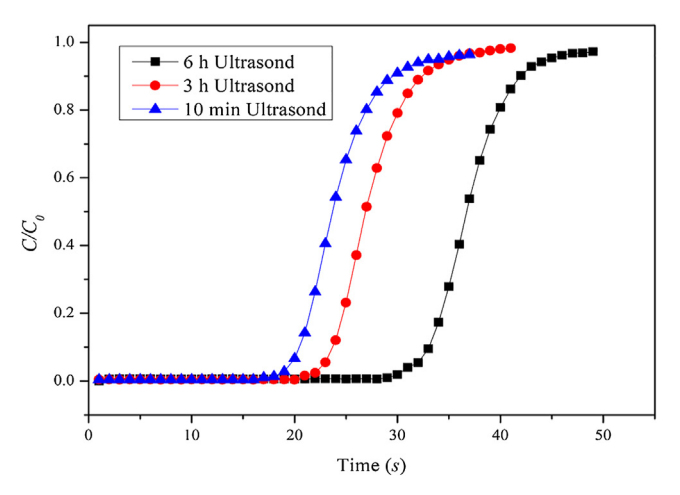


Fig. 8. Breakthrough curves of TEPA-GO.

Table 4 Adsorption capacity of TEPA-GO.

5–10 min Ultrasound 0.7	2–3 h Ultrasound 0.9	6 h Ultrasound 1.2	
Adsorption capacity at different temperatures (mmol ${\rm CO_2~g}^{-1}$ of adsorbent)			
303 K	323 K	338 K	
	0.7 Adsorption capacity at di adsorbent)	0.7 0.9 Adsorption capacity at different temperatures (madsorbent) 303 K 323 K	

^{*} Pristine GO was used without any ultrasound or chemical modification.

improved the CO_2 capture capacity of the graphene-based adsorbent. When GO was exposed to the ultrasonic irradiation, it exfoliated the graphene layers and made more room to attach functional groups to the matrix. The similar observation was also noted in our previous works [27,29]. The longer duration of ultrasound induced intense cavitation, and micro-jet formation that resulted to the higher exfoliation of the graphene layers. This substantially enhanced the surface area of the functionalized graphene and the number of amine functional groups attached to its structure. This induced the enhanced reaction between TEPA and GO surface functional groups and improved the adsorption capacity. Therefore, the activated sorbent with improved physico-chemical properties showed high sorption ability. The optimum sorption capacity of TEPA-GO is found to be 1.2 mmol g $^{-1}$ of adsorbent which is comparable to the literature [27].

The adsorption capacities of GO and TEPA-GO were compared with those values obtained for carbon adsorbents commonly found in the literature (Table 5). As observed, the ultrasonic-TEPA functionalized GO demonstrated a comparable adsorption capacity (1.2 mmol g⁻¹) with respect to EDA, DETA, TETA activated graphene oxides or PEI functionalized activated carbon. It is worth noting that the adsorption tests in this study were conducted using diluted CO2 with the partial pressure of 0.1 atm, however, most of the adsorption tests in the literature have used pure CO₂ with 1 atm or even higher pressures [51]. The adsorption capacity of functionalized GO from the present study is slightly lower than that for GO activated with APTES [52] and carboxyl-rich porous carbons activated with TEPA [53]. In the former case, the presence of silylating moieties are favorable for the covalent attachment of the functional groups to the support and thus improved sorption capacity [52]. And in the latter, the higher adsorption capacity attributes to the difference between the structure, surface area and porosity of GO and porous carbon and the presence of a high quantity of carboxylic groups in carbon structure, which further facilitates the process of amination [53] and that both tests were conducted under pure CO₂. Optimization of the ultrasonic-amination process along with

Table 5
Comparison of adsorption capacities of GO and TEPA-GO (present study) with literature.

Adsorbent	Activating Agent	Temp. K	CO ₂ Partial Pressure (bar)	${\rm CO_2}$ Adsorption (mmol.g $^{-1}$)	Ref.
GO	EDA, DETA, TETA	303	1	1.1	[54]
GO	3-aminopropyltriethoxysilane	298	2.1	3	[51]
GO	APTES	303	1	1.5	[52]
Graphite oxide	EDA	303	0.15	1.1	[26]
Carboxyl-rich porous carbons	TEPA	348	1	1.7	[53]
Fluorinated Graphene	EDA	273	1.1	1.16	[55]
Activated carbons	-	303	1	1.09	[56]
Activated carbons	PEI	333	1	1.23	[57]
GO	US-TEPA*	343	0.10	1.2	Present study
GO	-	303	0.10	0.3	Present study

^{*} US: ultrasound, the functionalization carried out in combination with ultrasound and TEPA activation.

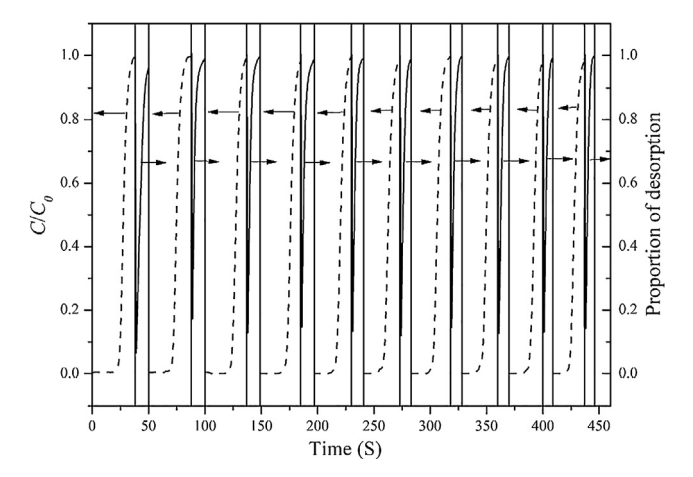


Fig. 9. CO₂ adsorption/desorption cycles of TEPA-GO.

conducting the tests under pure CO_2 can further improve the adsorption capacity of TEPA-GO.

3.9. The cyclic adsorption/desorption of TEPA-GO

Regeneration of the adsorbent is necessary from an economic point of view and for long-term use. Fig. 9 represents the breakthrough curves and the desorption curves of 10 adsorption/desorption cycles. The adsorption experiment (dash line) was carried out under 10 vol% CO2 and 90 vol% He at 338 K and the desorption experiment were conducted at 378 K under pure He flow (solid line). The cyclical adsorption/desorption data indicated that the adsorption behavior of the TEPA-GO was quite stable while the adsorption capacity decreased by only 1% after 10 cycles. However, a higher number of cyclical tests is needed for practical applications which may show further reduction in the adsorption capacity. Therefore, a suitable regeneration technique needs to be developed that will retain the adsorption capacity but at the same time should be feasible to conduct in terms of energy efficiency. This may be the motivation to direct the present work in future for the synthesis of suitable adsorbent and its regeneration for cyclic adsorption-desorption tests.

4. Conclusions

The present study investigates the effectiveness of the developed sono-chemical activation method for production of amine functionalized graphene oxide adsorbent for CO_2 capture. In this work, GO was prepared through the modified Hummer's method and then was subsequently functionalized by the augmented physical activation by ultrasound and chemical activation by TEPA in combination with EDC-HOBt as activating agents (highlight the steps and the process). The experimental results showed that the ultrasound irradiation was very

effective in exfoliating the graphene clusters and subsequent TEPA grafting through the interaction between the amine and the oxygen-containing groups of GO. The efficacy of the applied treatment was further confirmed through the characterization of TEPA-GO and the $\rm CO_2$ adsorption results. The improved $\rm CO_2$ capture capacity of the TEPA-GO was due to the interaction between the nucleophilic amines and the electrophilic $\rm CO_2$. The $\rm CO_2$ adsorption results also revealed that adsorption capacity increased with the sonication duration. The optimum adsorption capacity achieved by TEPA-GO was 1.2 mmol g $^{-1}$ of adsorbent at 338 K and 0.10 atm. partial pressure of $\rm CO_2$. Additionally, only 1% reduction in the sorption capacity after 10 cycles during the cyclic experiments demonstrated that the adsorption performance of TEPA-GO was quite stable. Hence, based on these results future work will be directed on 3D pore structure design to increase the adsorption rate and adsorption capacity of graphene composites

Acknowledgments

The authors are grateful to the Science Foundation of Fujian Province (Grant No. 2017J01472; No. 2017J01568; No. 2019J01061133) and the National Science Foundation (NSF EPSCoR RII Grant No. OIA-1632899) of the United States for financial support.

References

- Mac Dowell N, Fennell PS, Shah N, Maitland GC. The role of CO₂ capture and utilization in mitigating climate change. Nat Clim Change 2017;7(4):243.
- [2] Conti J, Holtberg P, Diefenderfer J, LaRose A, Turnure JT, Westfall L. International energy outlook 2016 with projections to 2040. Washington, DC (United States): USDOE Energy Information Administration (EIA); 2016.
- [3] Boot-Handford ME, Abanades JC, Anthony EJ, Blunt MJ, Brandani S, Mac Dowell N, et al. Carbon capture and storage update. Energy Environ Sci 2014;7(1):130–89.
- [4] Dhoke C, Zaabout A, Cloete S, Seo H, Y-k Park, Blom R, et al. The swing adsorption reactor cluster (SARC) for post combustion CO₂ capture: experimental proof-ofprinciple. Chem Eng J 2018.
- [5] Liu Z, Niu W, Chu H, Zhou T, Niu Z. Effect of the carbonization temperature on the properties of biochar produced from the pyrolysis of crop residues. BioResources 2018;13(2):3429-46.
- [6] Wang J, Huang L, Yang R, Zhang Z, Wu J, Gao Y, et al. Recent advances in solid sorbents for CO₂ capture and new development trends. Energy Environ Sci 2014;7(11):3478–518.
- [7] Kongnoo A, Tontisirin S, Worathanakul P, Phalakornkule C. Surface characteristics and CO₂ adsorption capacities of acid-activated zeolite 13X prepared from palm oil mill fly ash. Fuel 2017;193:385–94.
- [8] Klinthong W, Huang C-H, Tan C-S. Polyallylamine and NaOH as a novel binder to pelletize amine-functionalized mesoporous silicas for CO₂ capture. Microporous Mesoporous Mater 2014;197:278–87.
- [9] Lashaki MJ, Sayari A. CO₂ capture using triamine-grafted SBA-15: the impact of the support pore structure. Chem Eng J 2018;334:1260–9.
- [10] Chen C, Lee Y-R, Ahn W-S. CO₂ adsorption over metal-organic frameworks: a mini review. J Nanosci Nanotechnol 2016;16(5):4291–301.
- [11] Manyà JJ, González B, Azuara M, Arner G. Ultra-microporous adsorbents prepared from vine shoots-derived biochar with high CO₂ uptake and CO₂/N₂ selectivity. Chem Eng J 2018;345:631–9.
- [12] Álvarez-Gutiérrez N, Gil M, Rubiera F, Pevida C. Kinetics of CO2 adsorption on cherry stone-based carbons in CO2/CH₄ separations. Chem Eng J 2017;307:249–57.
- [13] Creamer AE, Gao B. Carbon-based adsorbents for postcombustion CO2 capture: a critical review. Environ Sci Technol 2016;50(14):7276–89.

- [14] Chen C, Huang H, Yu Y, Shi J, He C, Albilali R, et al. Template-free synthesis of hierarchical porous carbon with controlled morphology for CO₂ efficient capture. Chem Eng J 2018;353:584–94.
- [15] Gil A, Arrieta E, Vicente M, Korili S. Synthesis and CO₂ adsorption properties of hydrotalcite-like compounds prepared from aluminum saline slag wastes. Chem Eng J 2018;334:1341–50.
- [16] Fayemiwo KA, Vladisavljević GT, Nabavi SA, Benyahia B, Hanak DP, Loponov KN, et al. Nitrogen-rich hyper-crosslinked polymers for low-pressure CO₂ capture. Chem Eng J 2018;334:2004–13.
- [17] Jung H, Jeon S, Jo DH, Huh J, Kim SH. Effect of crosslinking on the $\rm CO_2$ adsorption of polyethyleneimine-impregnated sorbents. Chem Eng J 2017;307:836–44.
- [18] Chiang Y-C, Juang R-S. Surface modifications of carbonaceous materials for carbon dioxide adsorption: a review. J Taiwan Inst Chem Eng 2017;71:214–34.
- [19] Erickson K, Erni R, Lee Z, Alem N, Gannett W, Zettl A. Determination of the local chemical structure of graphene oxide and reduced graphene oxide. Adv Mater 2010;22(40):4467–72.
- [20] Dreyer DR, Park S, Bielawski CW, Ruoff RS. The chemistry of graphene oxide. Chem Soc Rev 2010;39(1):228–40.
- [21] Hofmann U, Holst R. Über die säurenatur und die methylierung von graphitoxyd. Berichte der deutschen chemischen Gesellschaft (A and B Series) 1939;72(4):754–71.
- [22] Chandra V, Yu SU, Kim SH, Yoon YS, Kim DY, Kwon AH, et al. Highly selective CO₂ capture on N-doped carbon produced by chemical activation of polypyrrole functionalized graphene sheets. Chem Commun 2012;48(5):735–7.
- [23] Li X, Cheng Y, Zhang H, Wang S, Jiang Z, Guo R, et al. Efficient CO₂ capture by functionalized graphene oxide nanosheets as fillers to fabricate multi-permselective mixed matrix membranes. ACS Appl Mater Interfaces 2015;7(9):5528–37.
- [24] Song Y, Cao L, Yu J, Zhang S, Chen S, Jiang Y. Amino-functionalized graphene oxide blend with monoethanolamine for efficient carbon dioxide capture. J Alloy Compd 2017;704:245–53.
- [25] Mishra AK, Ramaprabhu S. Carbon dioxide adsorption in graphene sheets. AIP Adv 2011;1(3):032152.
- [26] Zhao Y, Ding H, Zhong Q. Preparation and characterization of aminated graphite oxide for CO₂ capture. Appl Surf Sci 2012;258(10):4301–7.
- [27] Chen WY, Mattern DL, Okinedo E, Senter JC, Mattei AA, Redwine CW. Photochemical and acoustic interactions of biochar with CO₂ and H₂O: applications in power generation and CO₂ capture. AIChE J 2014;60(3):1054–65.
- [28] Stankovich S, Dikin DA, Dommett GH, Kohlhaas KM, Zimney EJ, Stach EA, et al. Graphene-based composite materials. Nature 2006;442(7100):282.
- [29] Chatterjee R, Sajjadi B, Mattern DL, Chen W-Y, Zubatiuk T, Leszczynska D, et al. Ultrasound cavitation intensified amine functionalization: a feasible strategy for enhancing CO₂ capture capacity of biochar. Fuel 2018;225:287–98.
- [30] Burress JW, Gadipelli S, Ford J, Simmons JM, Zhou W, Yildirim T. Graphene oxide framework materials: theoretical predictions and experimental results. Angew Chem Int Ed 2010;49(47):8902–4.
- [31] Bourlinos AB, Steriotis TA, Karakassides M, Sanakis Y, Tzitzios V, Trapalis C, et al. Synthesis, characterization and gas sorption properties of a molecularly-derived graphite oxide-like foam. Carbon 2007:45(4):852–7
- [32] Ma Y, Chen Y. Three-dimensional graphene networks: synthesis, properties and applications. Natl Sci Rev 2014;2(1):40–53.
- [33] Marcano DC, Kosynkin DV, Berlin JM, Sinitskii A, Sun Z, Slesarev A, et al. Improved synthesis of graphene oxide. ACS Nano 2010;4(8):4806–14.
- [34] Dimiev AM, Tour JM. Mechanism of graphene oxide formation. ACS Nano 2014;8(3):3060–8.
- [35] Tuinstra F, Koenig JL. Raman spectrum of graphite. J Chem Phys 1970;53(3):1126.
- [36] Zhao Q, Wu F, Xie K, Singh R, Zhao J, Xiao P, et al. Synthesis of a novel hybrid adsorbent which combines activated carbon and zeolite NaUSY for CO₂ capture by electric swing adsorption (ESA). Chem Eng J 2018;336:659–68.
- [37] Ferrari AC. Raman spectroscopy of graphene and graphite: disorder, electron-phonon coupling, doping and nonadiabatic effects. Solid State Commun

- 2007;143(1):47-57.
- [38] Nakamizo M, Honda H, Inagaki M. Raman spectra of ground natural graphite. Carbon 1978;16(4):281–3.
- [39] Oh J, Lee J-H, Koo JC, Choi HR, Lee Y, Kim T, et al. Graphene oxide porous paper from amine-functionalized poly (glycidyl methacrylate)/graphene oxide core-shell microspheres. J Mater Chem 2010;20(41):9200–4.
- [40] Liu J, Jeong H, Liu J, Lee K, Park J-Y, Ahn Y, et al. Reduction of functionalized graphite oxides by trioctylphosphine in non-polar organic solvents. Carbon 2010;48(8):2282–9.
- [41] Schniepp HC, Li J-L, McAllister MJ, Sai H, Herrera-Alonso M, Adamson DH, et al. Functionalized single graphene sheets derived from splitting graphite oxide. J Phys Chem B 2006;110(17):8535–9.
- [42] Zeng P, Zhang Q, Peng T, Zhang X. One-pot synthesis of reduced graphene oxide-cadmium sulfide nanocomposite and its photocatalytic hydrogen production. PCCP 2011:13(48):21496-502.
- [43] Sui Z-Y, Cui Y, Zhu J-H, Han B-H. Preparation of three-dimensional graphene oxide-polyethylenimine porous materials as dye and gas adsorbents. ACS Appl Mater Interfaces 2013;5(18):9172-9.
- [44] Hsiao M-C, Liao S-H, Yen M-Y, Liu P-I, Pu N-W, Wang C-A, et al. Preparation of covalently functionalized graphene using residual oxygen-containing functional groups. ACS Appl Mater Interfaces 2010;2(11):3092–9.
- [45] Dikin DA, Stankovich S, Zimney EJ, Piner RD, Dommett GH, Evmenenko G, et al. Preparation and characterization of graphene oxide paper. Nature 2007;448(7152):457.
- [46] McAllister MJ, Li J-L, Adamson DH, Schniepp HC, Abdala AA, Liu J, et al. Single sheet functionalized graphene by oxidation and thermal expansion of graphite. Chem Mater 2007;19(18):4396–404.
- [47] Juan Y, Ke-Qiang Q. Preparation of activated carbon by chemical activation under vacuum. Environ Sci Technol 2009;43(9):3385–90.
- [48] Sarkar C, Bora C, Dolui SK. Selective dye adsorption by pH modulation on aminefunctionalized reduced graphene oxide–carbon nanotube hybrid. Ind Eng Chem Res 2014;53(42):16148–55.
- [49] Xu C, Shi X, Ji A, Shi L, Zhou C, Cui Y. Fabrication and characteristics of reduced graphene oxide produced with different green reductants. PLoS One 2015;10(12):e0144842.
- [50] Yang T, L-h Liu, J-w Liu, Chen M-L, Wang J-H. Cyanobacterium metallothionein decorated graphene oxide nanosheets for highly selective adsorption of ultra-trace cadmium. J Mater Chem 2012;22(41):21909–16.
- [51] Bhanja P, Das SK, Patra AK, Bhaumik A. Functionalized graphene oxide as an efficient adsorbent for CO₂ capture and support for heterogeneous catalysis. RSC Adv 2016;6(76):72055–68.
- [52] Pokhrel J, Bhoria N, Anastasiou S, Tsoufis T, Gournis D, Romanos G, et al. CO₂ adsorption behavior of amine-functionalized ZIF-8, graphene oxide, and ZIF-8/ graphene oxide composites under dry and wet conditions. Microporous Mesoporous Mater 2018:267:53-67.
- [53] Zhao A, Samanta A, Sarkar P, Gupta R. Carbon dioxide adsorption on amine-impregnated mesoporous SBA-15 sorbents: experimental and kinetics study. Ind Eng Chem Res 2013;52(19):6480-91
- [54] Zhao Y, Ding H, Zhong Q. Preparation and characterization of aminated graphite oxide for CO₂ capture. Appl Surface Sci 2012.
- [55] Li B, Fan K, Ma X, Liu Y, Chen T, Cheng Z, et al. Graphene-based porous materials with tunable surface area and CO₂ adsorption properties synthesized by fluorine displacement reaction with various diamines. J Colloid Interface Sci 2016:478:36–45.
- [56] Younas M, Leong LK, Mohamed AR, Sethupathi S. CO₂ adsorption by modified palm shell activated carbon (PSAC) via chemical and physical activation and metal impregnation. Chem Eng Commun 2016;203(11):1455–63.
- [57] Wang P, Guo Y, Zhao C, Yan J, Lu P. Biomass derived wood ash with amine modification for post-combustion CO₂ capture. Appl Energy 2017;201:34–44.